Study of electrostatic distortions and possible corrections for a GEM based TPC readout module

Klaus Zenker, DESY, Hamburg, Germany

April 29, 2013

Abstract

In test beam data a partial reduced signal sensitivity of a GEM based readout module was observed. Electrostatic field simulations and subsequent electron drift studies to understand this problem were done and are presented here. It is shown, that distortions of the drift field introduced by the module itself can explain the observed effect. In addition, from the results of this study different possibilities of improvement are deduced and presented here. The presented approach to study field distortion is also applicable also to other problems.

1 Introduction

In July 2011 a *Time Projection Chamber* (TPC) prototype, called large TPC (LP)[1] [1, 2], was operated at DESY. For the operation described here electrons with a momentum of 5 GeV passed through the sensitive volume of the LP. The signals arising in the LP were detected by a GEM based readout module developed by the DESY TPC group. One result of this test beam was, that the module showed a reduced signal sensitivity at the borders of the module. This is inevitable in a modular TPC due to gaps between the modules. These gaps introduce distortions to the homogeneous drift field of the TPC. Thus it is essential to keep the distortions as low as possible to achieve an excellence performance of the TPC.

The aim of this work is to investigate distortions of the drift field in a modular read out and to find possible corrections. In doing so it should be possible to recover signal sensitivity of the readout module. First of all the experimental setup, including the readout module and the data analysis, is introduced in Section 2. Afterwards the electrostatic simulation used to understand the module behaviour is introduced in Section 3. Using the results of the simulation, various options to improve the module with regard to the signal sensitivity are presented and evaluated in Section 4. Besides the electrostatic simulation, in Section 5 the influence of a magnetic field is studied. A summary is presented in Section 6.
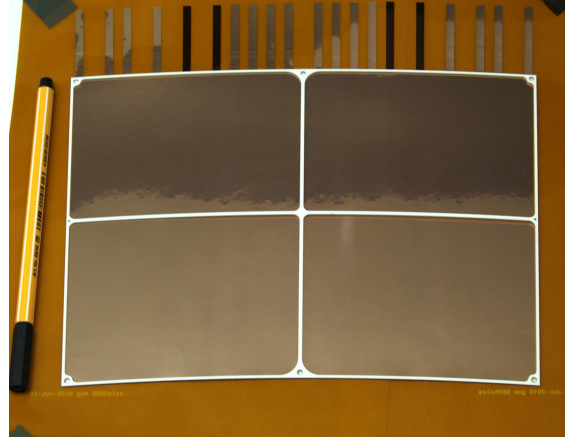
2 Experimental Setup

The setup used in July 2011 was placed in the DESY T24/1 test beam area, where electrons and positrons with a momentum of up to 6 GeV/c are available from the synchrotron DESY II [3]. The LP was inserted into a magnet, which allows to operate this TPC with and without a magnetic field of $B = 1$ T. Measurements and simulations presented here are without magnetic field, except the results shown in Sec. 5.
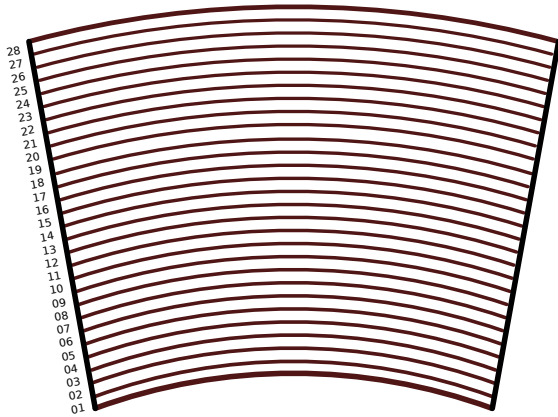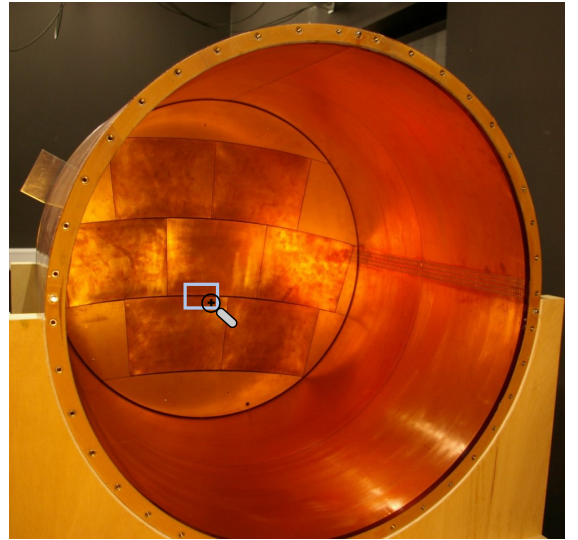
---

[1]Within the EUDET program the FLC TPC Group at DESY in collaboration with the Department of Physics of the University of Hamburg has constructed a large TPC prototype.
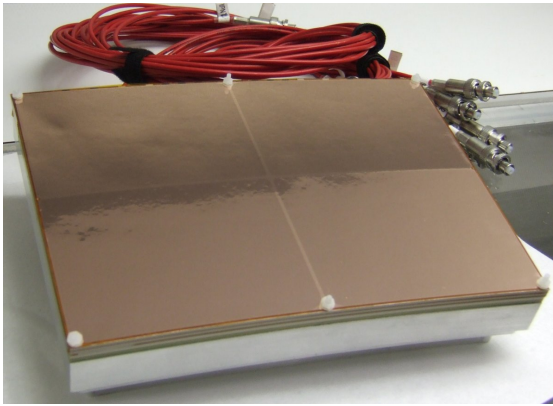
(a) Fully assembled module.   (b) Ceramic frame glued on a GEM.

Figure 1: Triple GEM module developed by the DESY TPC group

Figure 2: Sketch of the pad plane. Pads themselves are not shown.

Figure 3: Open field cage with removed cathode, so that the 7 dummy modules installed on the anode side are visible.

2.1   DESY module

The TPC readout module developed at DESY consists of three *Gas Electron Multiplier* (GEM) [4] foils acting as gas amplifier structure, shown in Fig. 1(a). One feature of this module is the use of ceramics glued to the GEMs, shown in Fig. 1(b). These ceramics are used to separate the GEMs and allow to reduce the sagging of GEM foils without covering much of the sensitive area [5]. The charge is collected on sensitive pads $\left(1.26 \times 5.85\,\mathrm{mm}^2\right)$ arranged in 28 rows, of which the first one is at the bottom of the module. A sketch of pad plane is shown in Fig. 2. The number of pads, which are not shown in this sketch, varies with the row number due to the constant pad size.

In Fig. 3 the anode of the LP with 7 dummy modules installed, forming a copper surface at the end of the drift volume, is shown. During test beam operation the central dummy module was replaced by the read out module introduced above.
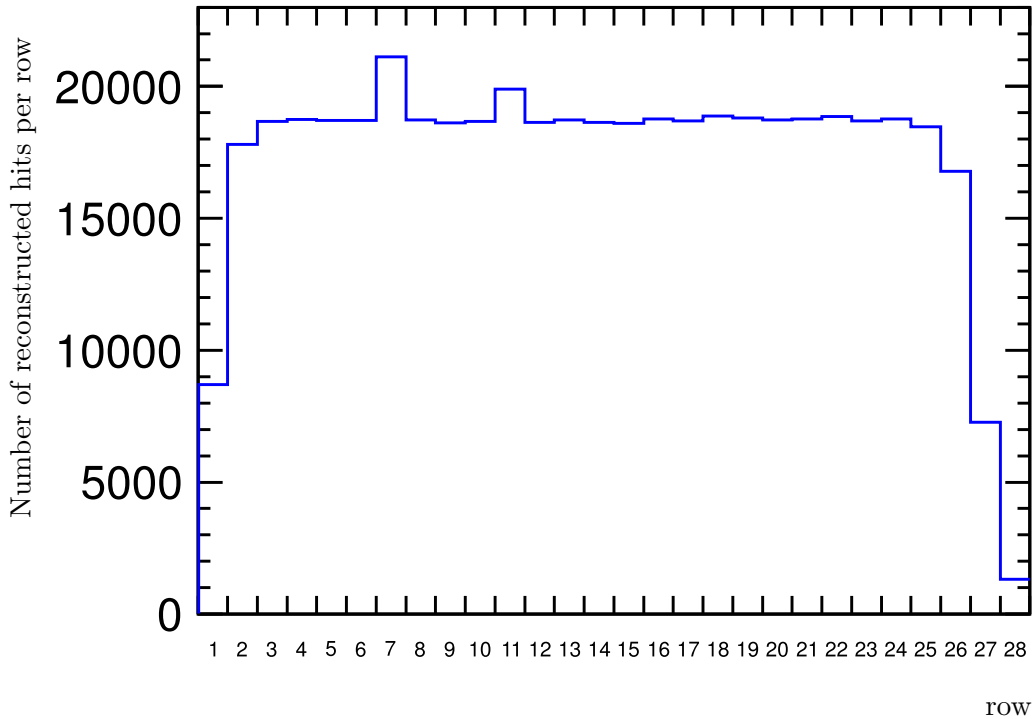
Figure 4: Test beam result from July 2011 showing a decreased number of reconstructed hits per row at the border of the readout module. This measurement was taken without a magnetic field.

2.2   Data analysis

The data taken during test beam were reconstructed with the software MarlinTPC [6, 7] up to the hit level. No fitting was applied. The resulting number of hits per row is shown in Fig. 4.

There are two rows, which collected significant more hits compared to all other rows. This effect is understood and can be explained by pads in these rows which could not be read out. For this reason, the hit finding algorithm reconstructs one signal pulse as two hits in this row – one hit left to the dead pad and one hit right to the dead pad. Furthermore, comparing the number of hits collected at the borders of the module (row 1-2 and 26-28 respectively) and the central part of the module (row 4-23), it can be seen that the number of reconstructed hits is reduced. One reason for this effect appearing at the borders of the module is most likely field distortions introduced by the gap between the module and the neighbouring dummy modules.

In more detail, Fig. 4 shows that on the upper part of the module three rows are affected, whereas at the bottom only two rows are affected. This is consistent with the fact, that the gap between the module and the neighbouring dummy module is larger on the top (2 mm). A larger gap introduces larger field distortions. In addition on top the high voltage is routed to the GEMs, which introduces additional field distortions.

In order to study the field distortions a simulation, introduced in the following, is performed. In this simulation we only concentrate on understanding the distortions due to the geometry of the module leaving out all other effects like the HV routing, which might influence the performance of the readout module. Thus the bottom part, where the gap between the module and the neighbouring dummy module is 1 mm, defined the overall geometry for the simulation.
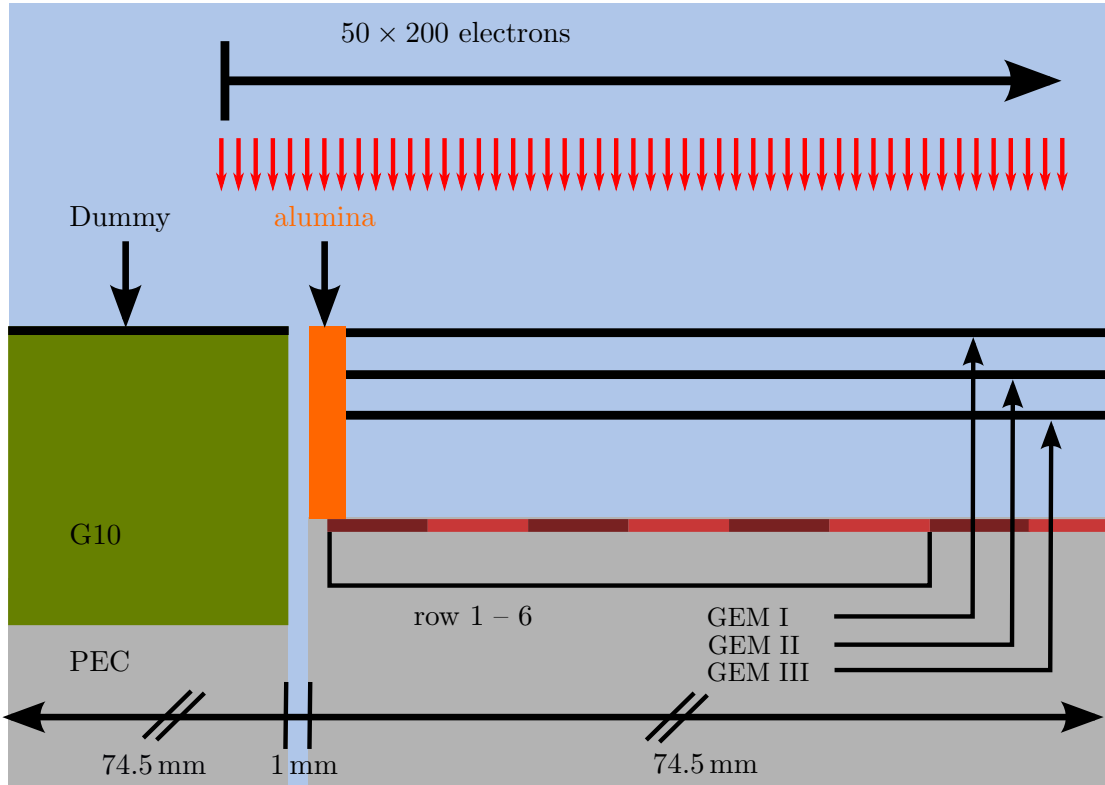
Figure 5: Model of the DESY module used for field calculations in CST™ (side view). The red arrows on top show the start points of the electrons as used in the GARFIELD++ simulation. The light blue area represents the drift volume filled with T2K gas in the GARFIELD++ simulation.

3 Simulation

In this section the electrostatic field distortions appearing in a homogeneous field by a gap in a conductive surface are investigated. This is a simplified model of the problem explained in the previous section, which is introduced in Sec 3.1.

After defining the model of the module, the simulation will be explained. It is divided into two parts. First, an electrostatic simulation using a finite element based software is performed (Sec. 3.2). In the next step (Sec. 3.3), the information of the electric field is used to drift electrons from the drift volume towards the module. Afterwards, the electrons endpoints are analysed. By comparing the start and end position of the electron, the displacement due to field distortions can be evaluated.

3.1 The model

The model used for the simulations deals with a small cut-out of the region where the dummy module and the readout module are next to each other (see light blue box in Fig. 3). This region is modelled as two copper surfaces, each with a length of 74.5 mm, representing the dummy module and the GEM surface on top of the GEM stack. In the following these surfaces will be referred to as Dummy and GEM I. Between both surfaces there is a gap of 1 mm. Above the surfaces a volume representing the drift volume with a height of 25 mm is modelled, corresponding to the maximum drift length. A side view of the model is shown in Fig. 5. Here it can be seen, that the dummy module (left-hand side) and the read out module (right-hand side) are also modelled below the surfaces mentioned before. Thus, on the right-hand side in Fig. 5, the pad rows of the

Table 1: Potentials applied in the simulation.

volume	potential
PEC	0 V
GEM III	-1200 V
GEM II	-1800 V
GEM I	-2200 V
Dummy	-2200 V
boundary (at z_{max})	-2750 V

pad plane can be seen. The ceramic structure supporting the GEMs is modelled with aluminium and shown in orange.

In total, four different kinds of material, characterised by different permittivities, are used in the simulation:

- G10

- alumina with a purity of 96 % (CeramTech Rubalit® 708S[8])

- perfect electric conductor (PEC)

- copper

The drift volume and the volume in the gap is filled with vacuum in the electrostatic field simulation. In Table 1 the potentials used in the simulation are presented. By applying these potentials, a homogeneous field in the drift region of $E_{\text{drift}} = 220$ V/cm is intended and formed between the boundary of the simulation and the surfaces (Dummy and GEM I).

3.2   Electrostatic field simulation

The electrostatic field simulation is done with the software CST Studio Suite™ [9]. Field calculations with CST™ make use of finite elements and Maxwell's equation in their integral form [10]. In the simulation a hexahedral mesh with about 7 million elements of different size is used. The mesh size is smaller in the vicinity of the gap between the Dummy and GEM I. In the drift region field variations are expected to be smaller and thus the mesh size is larger. In addition an algorithm for treating material boundaries which cannot be modelled with cubes of the hexahedral mesh, called *Perfect Boundary Approximation* (PBA) algorithm, was used (see [11]).

For the given potentials (Table 1) the result of the simulation is shown in Fig. 6. Here the field component transverse to the drift field is shown. In the drift area above the GEM the transverse field component is smaller than the drift field $E_{\text{drift}} = 220$ V/cm. But in the vicinity of the gap between the Dummy and GEM I the transverse field component exceeds 500 V/cm. Thus the simulation shows, that distortions can be traced back to the gap between the two surfaces (Dummy and GEM I) put on the same potential. This distortion of the drift field clearly has an effect on electrons drifting towards the read out module. In the next Section these distortions will be quantified further. Moreover, in Fig. 6 there are also field distortions affecting the volume within the GEM stack, affecting the avalanche process. These distortions are not within the scope of this work, but might be of interest in future studies.
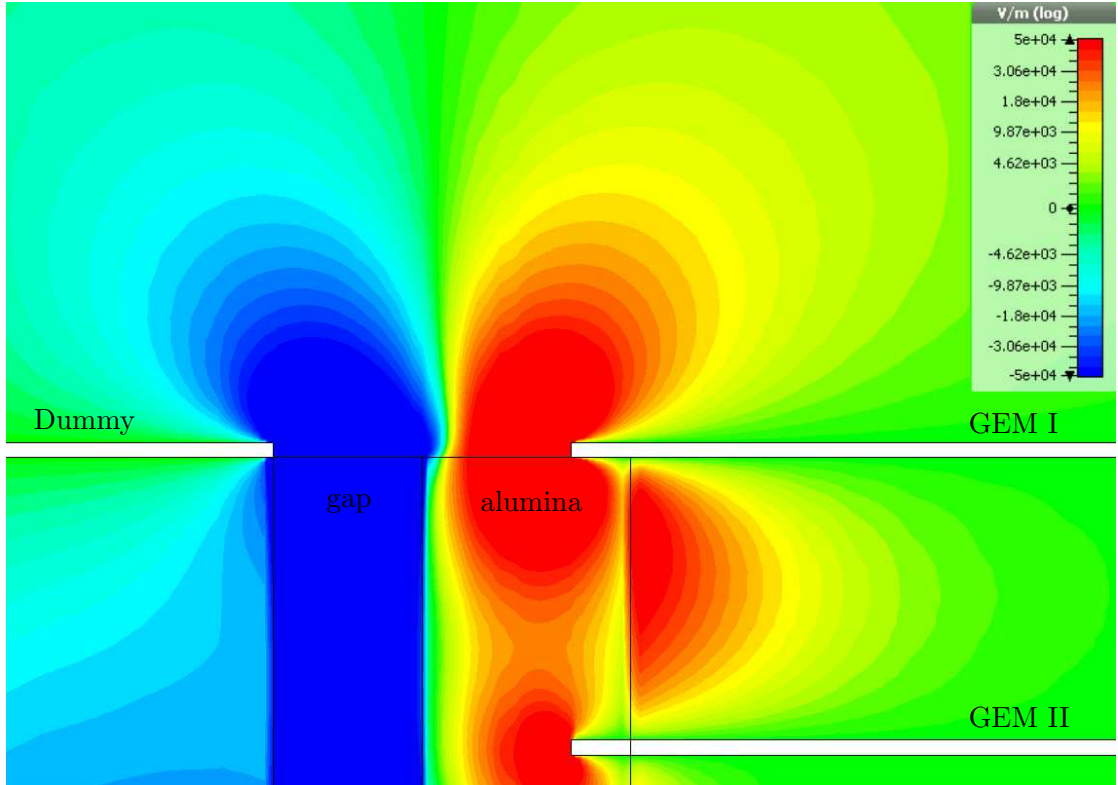
Figure 6: Simulation of the electric field component transverse to the drift field for the readout module without modification.

3.3   Electron drift studies

In order to simulate the electron drift the program GARFIELD++ [12, 13] is used. It treats ionisation processes and the transport of charged particles in gases. A detailed description of the performed drift simulation is given in the following.

Electron drift

The gas, known as T2K gas, used in the simulation and during the test beam is a mixture of 95 % Ar, 3 % CF_4 and 2 % iC_4H_{10}. Initially one electron is released above the module in the drift volume from one start point. Subsequently it drifts towards the module following the drift field. If an electron reaches the modelled surfaces (Dummy and GEM I) or the gap between these surfaces, the drift is stopped and the current position of the electron is stored. Thus it can be decided if the electron was stopped on the Dummy surface, the GEM I surface or on top of the gap. Furthermore, by projecting the row positions on the GEM I surface, it can be estimated on which row the electron would have been recorded in the experiment. This makes it possible to compare the number of electrons collected on a certain row with the number of hits reconstructed on a certain row in the experimental data.

This approach neglects all effects appearing in the GEM stack and that are related to the avalanche process or field distortions within the stack. Also, neither amplification or digitisation of the signal nor reconstruction algorithms where applied to the results. Thus the simulation only allows a qualitative comparison.

Signal modelling

In order to generate a signal on the row positions, not only one electron is released in the drift volume, but 200 electrons (N_{e^-}). These electrons follow different paths during the drift, since diffusion is taken into account by GARFIELD++. Without distortions of the drift field the endpoints are distributed following a 2D Gaussian distribution, where the centre of this distribution is equivalent to the start position and the variance is determined by the transverse diffusion.

In order to compare the simulation with the experimental results shown in Sec. 2, it is necessary to simulate a uniform electron cloud in the drift region. Then, without distortions of the drift field, one would get the same number of electron endpoints on each row . To achieve such a uniform distribution 50 equidistant start positions (N_{start}), 25 mm above the Dummy and GEM I surfaces (d_{drift}), are used. This is shown in Fig.5, where small arrows depict the start positions of the electrons. The first start position is 4.5 mm in front of the gap and thus above the Dummy surface. The distance between the start positions is 0.1 mm. Hence the last start position is 44.5 mm away from the gap and above the GEM I surface. This position corresponds to a start position above row 8 since each row has a width of $w_{\text{row}} = 5.85$ mm and the first row is 1 mm away from the gap.

In the following two cases are distinguished:

1) The electron endpoint position is in front of the first row (1 mm away from the gap).

2) The electron endpoint position is associated to one of the first six rows.

If a uniform electron cloud is achieved and there are no distortions of the drift field, the same number of electrons should be associated to each row (1-6, case 2). Furthermore more electrons than associated to each row should fulfil case 1, since the distance of the first start position to the first row is large compared to the distance between start positions. Thereby it is guaranteed, that the region of interest (row 1-6) is not influenced by effects corresponding to the margin of the electron cloud.

Expected signal on a certain row

Considering the signal generation as described in the previous section it is possible to calculate the expected signal for all three cases mentioned above. The transverse diffusion of the electrons in one dimension can be characterised by a Gaussian distribution, where the mean corresponds to the start position and the variance (σ^2) depends on the drift distance. Knowing the transverse diffusion of the drift gas it is possible to calculate σ from:

$$D = \frac{\sigma}{\sqrt{d_{\text{drift}}}}. \tag{1}$$

With GARFIELD++ it is possible to calculate the diffusion using the interface to Magboltz[14]. For T2K gas, an electric field of $E_{\text{drift}} = 220$ V/cm at $T = 293.15$ K and $p = 760$ Torr the diffusion is:

$$D(B = 0\,\text{T}) = (0.031 \pm 0.001)\,\text{cm}^{1/2} \tag{2}$$
$$D(B = 1\,\text{T}) = (0.0093 \pm 0.0002)\,\text{cm}^{1/2} \tag{3}$$

Here the magnetic field of 1 T was set parallel to the electric field.

In order to calculate the number of electrons ending on a certain row ($\tilde{N}_{\text{row}}$) the probability for each start point (x_{start}) needs to be summed up and multiplied by the number of electrons started

from this point. This leads to:

$$\tilde{N}_{\mathrm{row_i}} \;=\; N_{\mathrm{e^-}} \sum_{\mathrm{j=1}}^{N_{\mathrm{start}}} \int_{x_{\mathrm{min}}^{j}}^{x_{\mathrm{max}}^{j}} \frac{1}{\sqrt{2\pi}\sigma} \exp\left(-\frac{1}{2}\left(\frac{x - x_{\mathrm{start}}^{j}}{\sigma}\right)^{2}\right) dx, \tag{4}$$

where x_{min}^{j} and x_{max}^{j} correspond to the borders of the j-th row. In order to get the expected number of electrons for the case 1) discussed above one needs to adjust the bounds of the integral:

$$\tilde{N}_{\mathrm{underflow}} \;=\; N_{\mathrm{e^-}} \sum_{\mathrm{j=1}}^{N_{\mathrm{start}}} \int_{-\infty}^{x_{\mathrm{first}}^{j}} \frac{1}{\sqrt{2\pi}\sigma} \exp\left(-\frac{1}{2}\left(\frac{x - x_{\mathrm{start}}^{j}}{\sigma}\right)^{2}\right) dx. \tag{5}$$

In the following the number of electrons obtained in the simulation ($N_{\mathrm{row_i}}$, $N_{\mathrm{underflow}}$) is always normalised to the corresponding expected number of electrons:

$$n_{e^-,\mathrm{row}_i} \;=\; \frac{N_{\mathrm{row}_i}}{\tilde{N}_{\mathrm{row}_i}} \tag{6}$$

$$n_{e^-,\mathrm{underflow}} \;=\; \frac{N_{\mathrm{underflow}}}{\tilde{N}_{\mathrm{underflow}}} \tag{7}$$

Results of the drift study

The electron drift for two different start positions is shown in Fig. 7. It is clearly visible, that electrons started at position 1 are influenced by field distortions and guided towards the gap between the modelled surfaces (Dummy and GEM I). Such distortions are also visible for electrons started at position 2, but the influence is much smaller and the distortions introduced by the gap almost vanish. Therefore approximately the endpoint distribution appears to be caused by diffusion only.

Results of the drift simulation are shown in Fig. 8. Here the number of electrons stopped at a position corresponding to a certain row N_{row} normalised to the expected number of electrons stopped at this row $\tilde{N}_{\mathrm{row}}$, as introduced in the previous section, is shown. Underflow means that the electrons are stopped in front of the first row and thus correspond to case 1 introduced in the previous section.

In the region of interest, a reduced signal on row 1 is clearly visible in Fig. 8. Therefore the general feature seen in the experiment, that mainly the first row is effected by field distortions, is reproduced qualitatively in the simulation. Compared to the experimental result of approximately 47% at row 1 the obtained result shows a lower reduction of the signal collection of 63%. This difference between the simulations including the uncertainties and the experimental results can be assigned to the simplified model used here. The uncertainties given in Fig. 8 and the following plots correspond to $\sqrt{N_e}$, assuming a Poisson distribution. A consistency check of the uncertainties is presented in Section 5.

Since the qualitative reproduction of experimental results was successful, different options to reduce the field distortions can be tested and are presented in the following.

position 1   position 2

GEMs
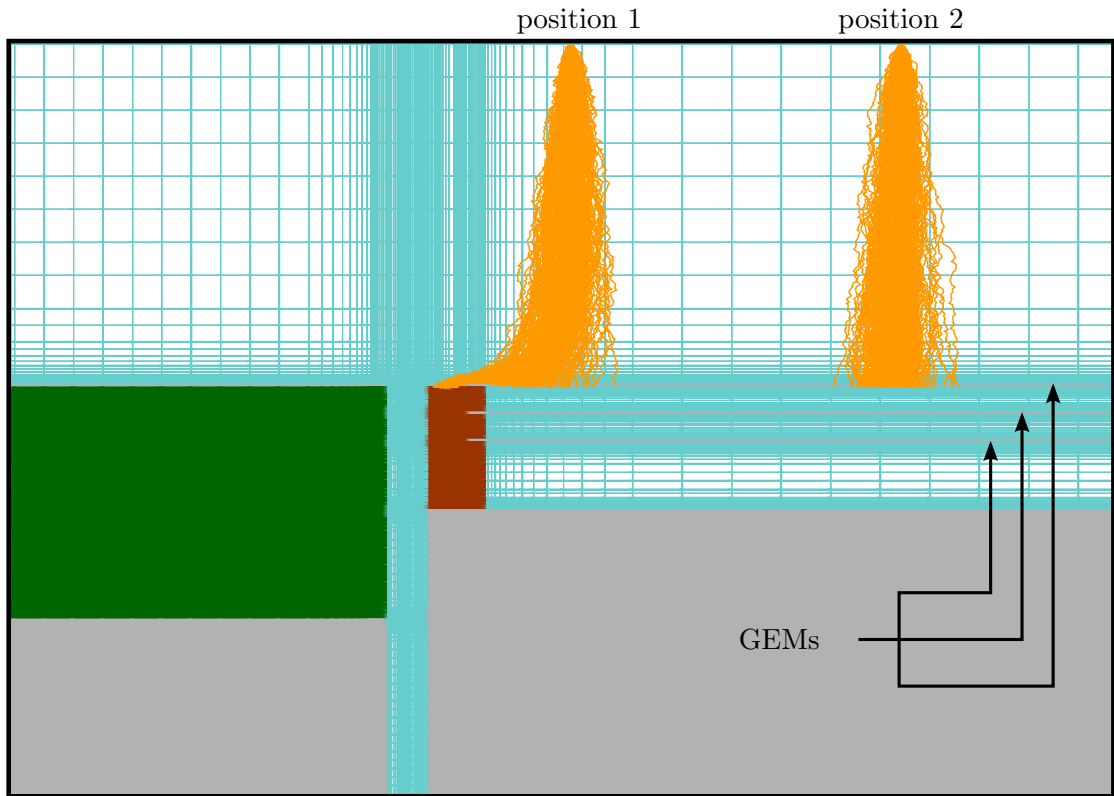
Figure 7: Electrons, started at two different start positions and represented by orange lines, drift towards the module (side view). Coloured boxes represent the mesh elements in the drift volume. PEC material is shown in grey, alumina in brown and G10 in green.
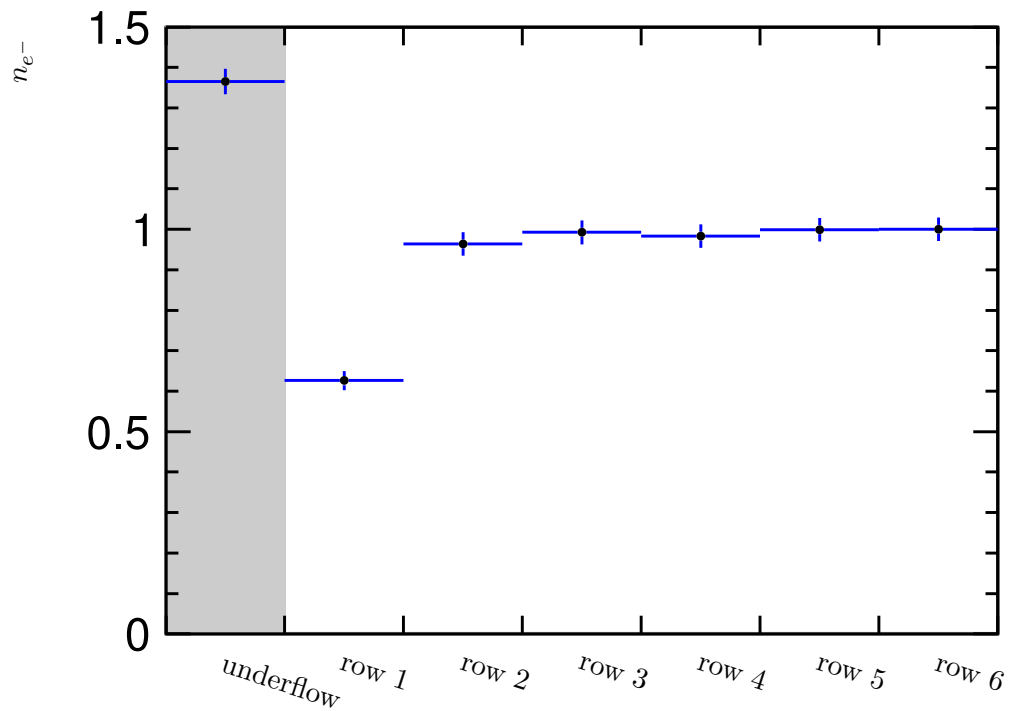
Figure 8: Number of electrons on a certain row position normalised to electrons on row 6.

4   Module optimisation

In order to reduce field distortions discussed in the previous sections, there are two fundamental approaches:

1. Close the gap between the Dummy and DESY module

2. Shape the field in the vicinity of the gap between the Dummy and the DESY module

The first approach is ruled out by experimental requirements. Thus, here only the second approach is considered. Several options of following this approach were considered and are introduced in the following. All of them are motivated by the feasibility on the experimental side.

First, on the surface of the ceramic frame introduced in Sec. 2.1, material can be added to shape the electric field. One option is to uniformly coat the external surface of the ceramics with a conductive material, resulting in a strip. The height of this strip is defined by the height of the ceramic frame which is 1 mm. In the simulation the strip is modelled as a 100 µm thick copper layer resulting in strips of the size 1 mm × 100 µm. Two different variations of this approach are tested:

one strip: The topmost ceramic frame is covered with copper.

two strip: The second and fourth ceramic frame, counted from top, is covered with copper.

In addition different voltages are applied. This is summarised in Table 2.

Another possibility is to attach a thin conductive wire to the middle of the topmost ceramic frame. Here wires with different diameters d and field configurations are used, which are also shown in Table 2.

In the case that one strip or a wire is attached to the ceramic frame, the distance to the top of the GEM stack is small. Thus, an approach, easy to realise in the experiment, is to apply the same potential as used for the topmost GEM ($U = -2200$ V, option a). The advantage is that no additional potential has to be provided. The second considered potential for the wires given in Table 2 (option b) corresponds to the idea of continuing the drift field in the gap between the Dummy and the readout module. In case of two strips this idea is realised in option a. Contrary to this, option b in Table 2 of the module with two strips uses an inverted drift field in the gap.

All analysis steps as presented in Sec. 3 were performed for each options described above. The results are presented in the following.

## 4.1   Results of the electrostatic field simulation

Selected results of the field simulations are shown in Fig. 9. Other results can be found in the appendix (Fig. 17,15). Judging from the field simulations, the field distortions can be reduced with both approaches (wire and strip). Comparing both approaches, the idea of adding a strip reduces distortions of the drift field more efficiently. One interesting feature in Fig. 9(b) is, that the transverse field component within the GEM stack is inverted compared with the default module and the wire modification.

4.2   Results of the electron drift simulation

In order to compare different options more quantitatively, drift studies (introduced in Sec. 3.3) are performed and presented in the following. It turned out that the difference between the
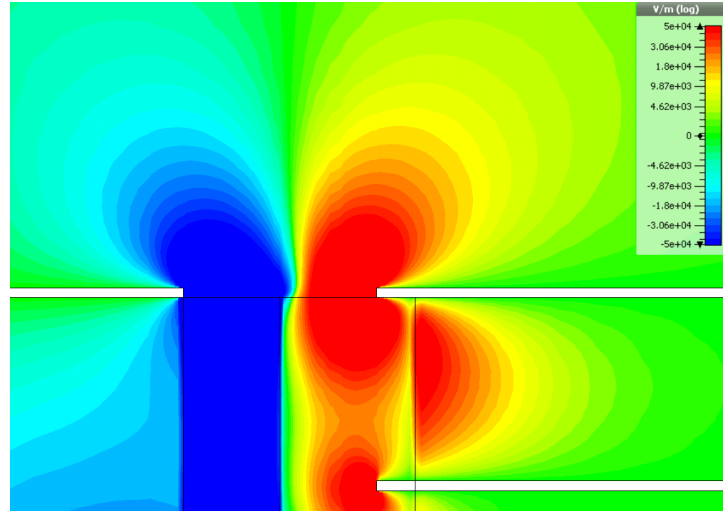
(a) Readout module without modifications.
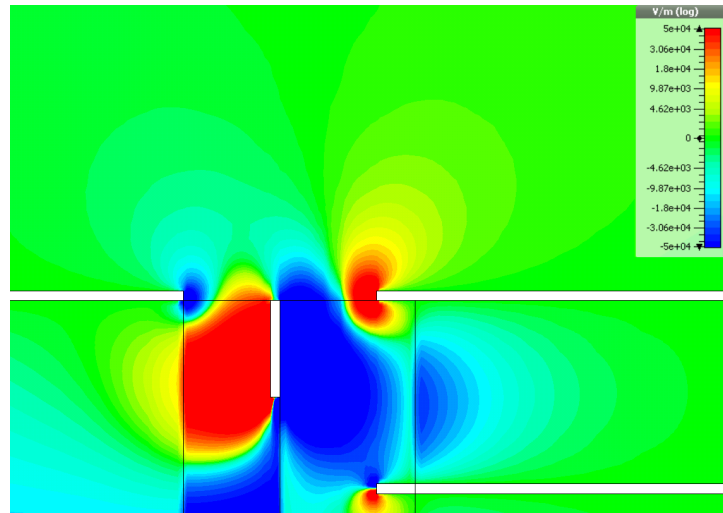
(b) Readout module with one strip at a potential of $U_{\text{strip}} = -2200\,\text{V}$.
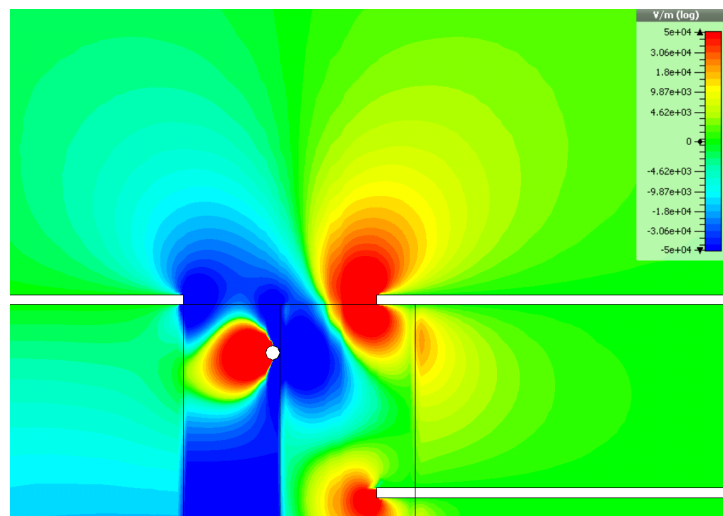
(c) Readout module with one wire $(150\,\mu\text{m})$ attached. The potential on the wire is $U_{\text{wire}} = -2200\,\text{V}$.

Figure 9: Different versions of the readout module. Shown is the electric field transverse to the drift field.

Table 2: Different wire and strip options and the corresponding potentials applied in the simulation.

	potential	
	option a	option b
wire ($d = 50\,\mu$m)	-2200 V	-2189 V
wire ($d = 100\,\mu$m)	-2200 V	-2189 V
wire ($d = 150\,\mu$m)	-2200 V	-2189 V
one strip	-2200 V	
two strips:		
top strip	-2167 V	-2233 V
bottom strip	-2123 V	-2277 V

introduced wire options is rather small as can be seen in the appendix (Fig. 19). In principle, wires with a larger diameter can reduce the distortions of the drift field more efficiently. The differences between the applied potentials are negligible taken the uncertainties into account. Also the results obtained when adding strips to the module are rather similar (see Fig. 18). Thus only results for the best and worst of each modification are presented here. In particular these are:

best strip: one strip

worst strip: two strip (option a)

best wire: $d = 150\,\mu$m, $U_{\text{wire}} = -2200\,$V (option a)

worst wire: $d = 50\,\mu$m, $U_{\text{wire}} = -2200\,$V (option a)

The results of the drift studies are shown in Fig. 10. Here it is clearly visible, that the number of electrons collected on row 1 can be increased with any of the modifications tested here. Thus less electrons are guided into the gap between the Dummy surface and the GEM I surface and therefore a better performance of the readout module is expected. More in detail, adding strips to the module leads to a higher number of electrons on row 1.
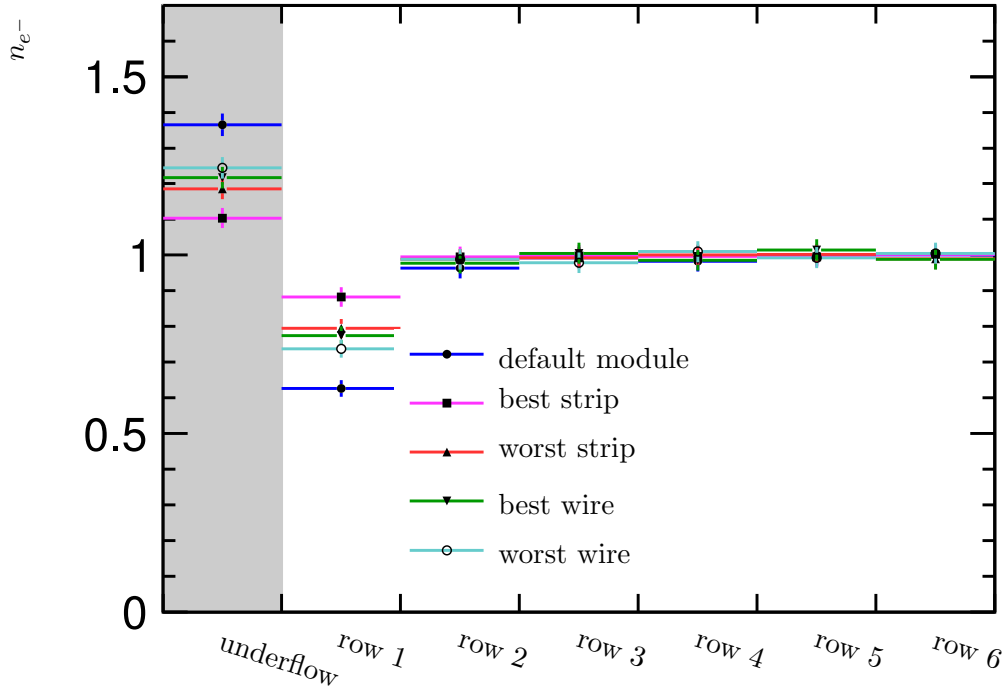
Figure 10: Number of electrons on a certain row position normalised to the expected number of electrons. Results for different possibilities of modifying the readout module are shown.

5 Influence of a magnetic field and uncertainty estimation

In this section the influence of a magnetic field is studied. This is done for the four modifications considered in the previous section and the default readout module. Since it is possible to operate the LP with a magnetic field of up to $B = 1\,\mathrm{T}$, this field strength was applied in the simulation. From theory (see e.g. [15]) it is known that for such a high magnetic field, electrons tend to follow the magnetic field lines. Since the magnetic field is applied in drift direction the influence of the electric field distortions is expected to be reduced in that sense it is discussed here. Emerging $\vec{E} \times \vec{B}$ effects of course have a big influence on the performance of the readout module, but here they are not investigated in detail.

In Fig. 11 the resulting n_{e^-} with magnetic field is shown. In agreement with the expectation, clearly an increased number of electrons in row 1 is visible compared to the results without magnetic field shown in Fig. 10.

Uncertainty estimation

A different approach than that one introduced in Sec. 3.3 to estimate uncertainties is presented here. The idea is to simulate two independent samples of the same size. Afterwards these samples are analysed in a similar way as done before. Finally the difference of n_{e^-} in each bin between these two samples is considered as an estimate of the uncertainty in that bin. The error bars in Fig. 12 depict the resulting uncertainties. In this figure the left axis shows the difference between n_{e^-} for the default readout module and modified versions of the module. Only the number of electrons on row 1 is considered since the modifications mostly effect this row. Contrary to the
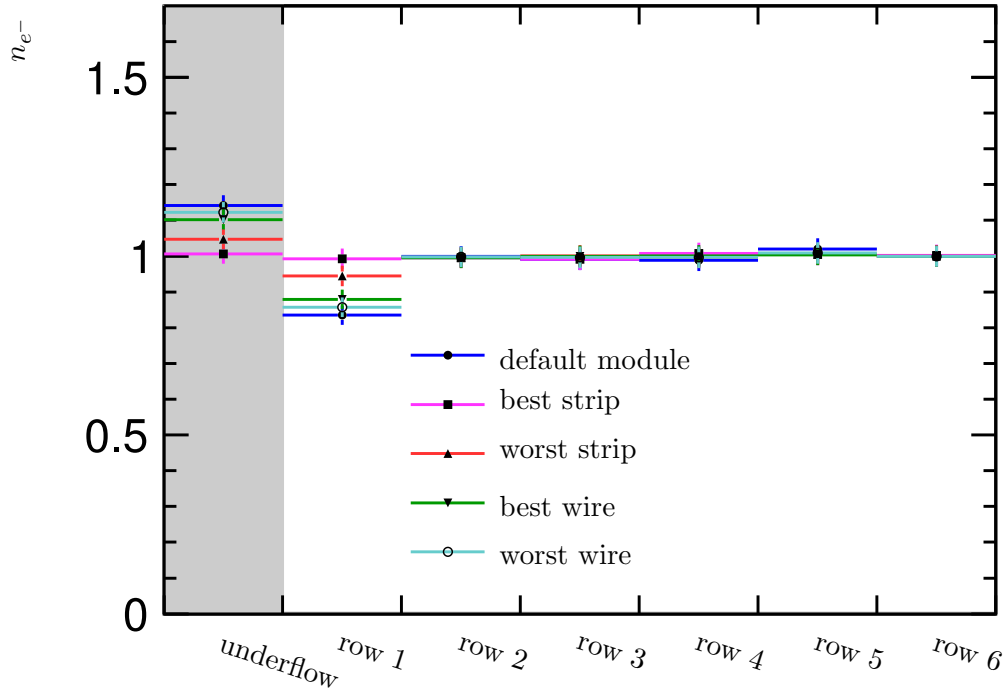
Figure 11: Number of electrons on a certain row position normalised to the expected number of electrons. Results for different possibilities of modifying the readout module are shown. A magnetic field of $B = 1\,\mathrm{T}$ parallel to the drift field was applied.

relative comparison with the default readout module on the left axis, the right axis shows the absolute value of n_{e^-} for row 1. Thus the bottom of this axis always corresponds to the result of the default module. Again it should be stressed that the results in Fig. 12(b) seem to show that the field distortions of the drift field nearly vanishes, but additional undesirable effects introduced by the magnetic field probably exist and are not visible in this analysis.

The uncertainties obtained using the method presented here, are of the same order as the uncertainties quoted in the previous sections. Thus both methods are suited to estimate the uncertainties and the assumptions concerning the uncertainties made in Sec. 3.3 are valid.
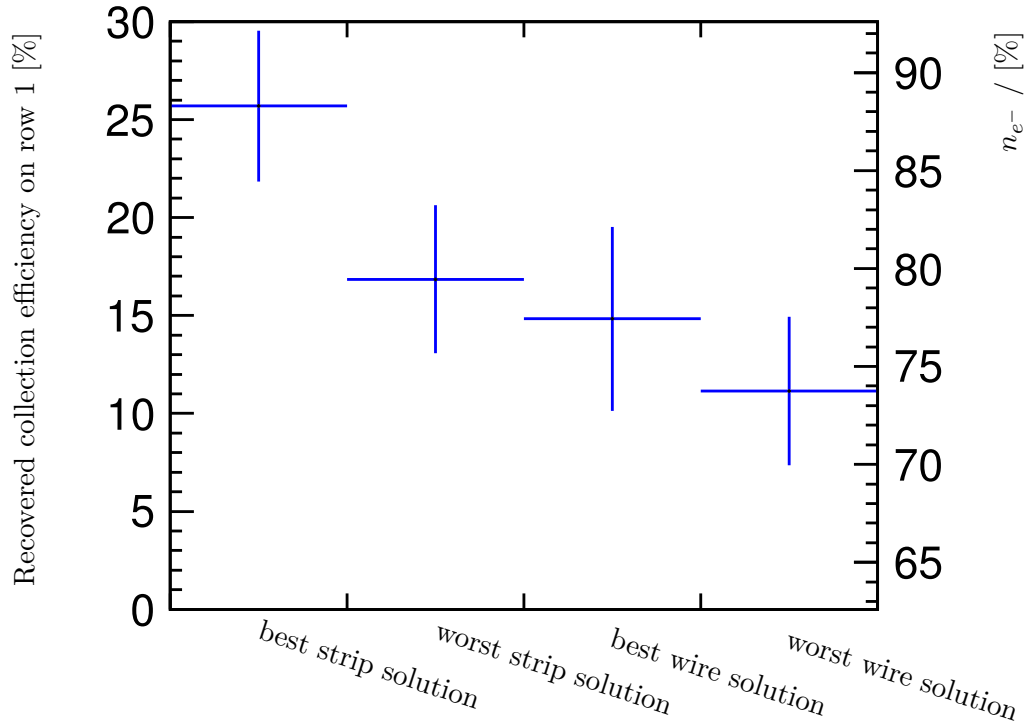
(a) No magnetic field is applied.
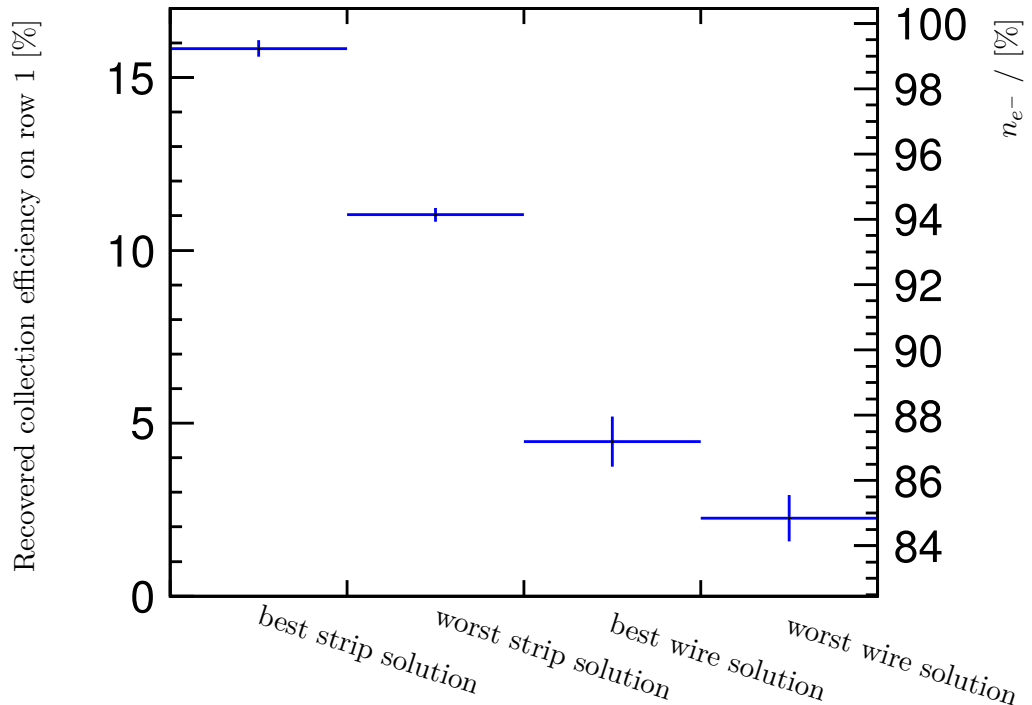
(b) A magnetic field of $B = 1\,\mathrm{T}$ in drift direction is applied.

Figure 12: Difference between the default readout module and modified versions of the module of the collection efficiency on row 1. Only the best and the worst option of different types of modification are shown. $0\,\%$ on the left scale corresponds to the default module. The right axis shows the absolute collection efficiency which allows to read also the result for the default readout module.

15

6 Summary

Electrostatic field simulations with CST™ and subsequent drift simulations with GARFIELD++ were used to understand the charge collection measured with a TPC module prototype. In simulation a reduced signal sensitivity near the border of the readout module could be reproduced. Also field distortions within the readout module, caused by its geometry and not investigated here, were observed and might be of interest in future studies. Furthermore different options to recover signal sensitivity were studied. The best option turned out to be a copper strip attached to the module which is connected to the cathode potential of the GEM facing the drift volume. Thus a collection efficiency of 88 % could be reached, which is 25 % higher with respect to the default readout module. Attaching a wire to the module also recovers the signal sensitivity with respect to the default module, but it is less efficient than attaching a strip. A summary of the results is shown in Fig. 13, where the difference between the default module and the modified module is shown. In addition the influence of magnetic field parallel to the drift field was investigated. It was shown that the magnetic field further reduces the effects of field distortions. Probably introduced $\vec{E} \times \vec{B}$ effects degrading the performance of the readout module are not discussed here and need further investigation.

The results of upcoming test beam campaigns will be used to check the results obtained here.
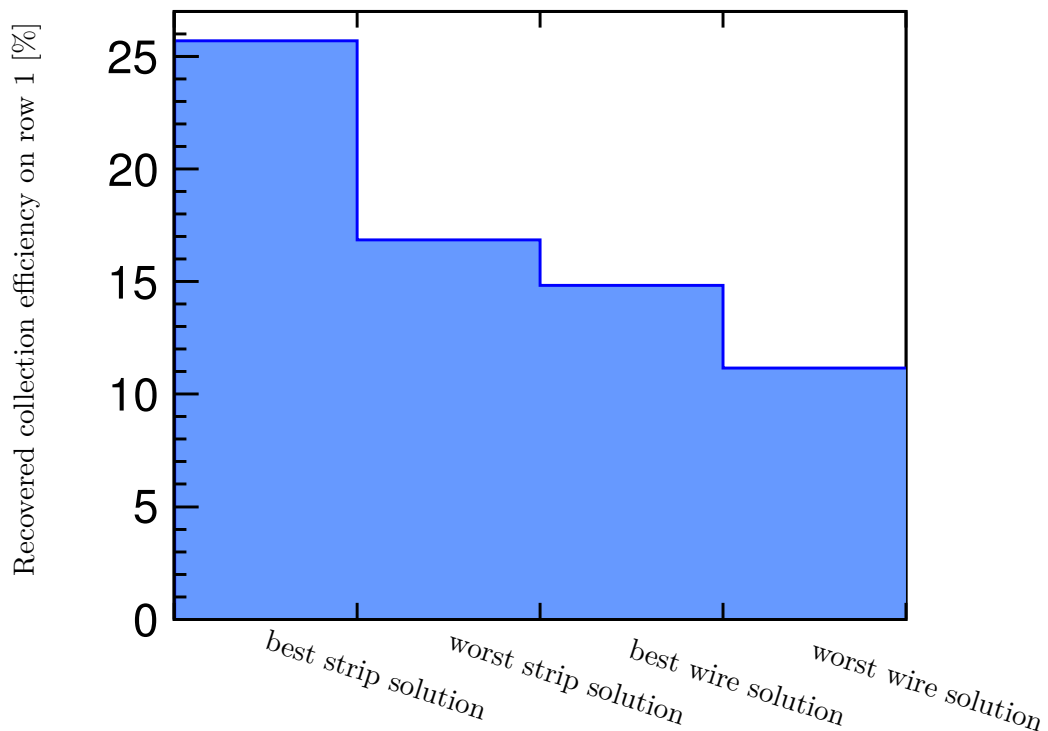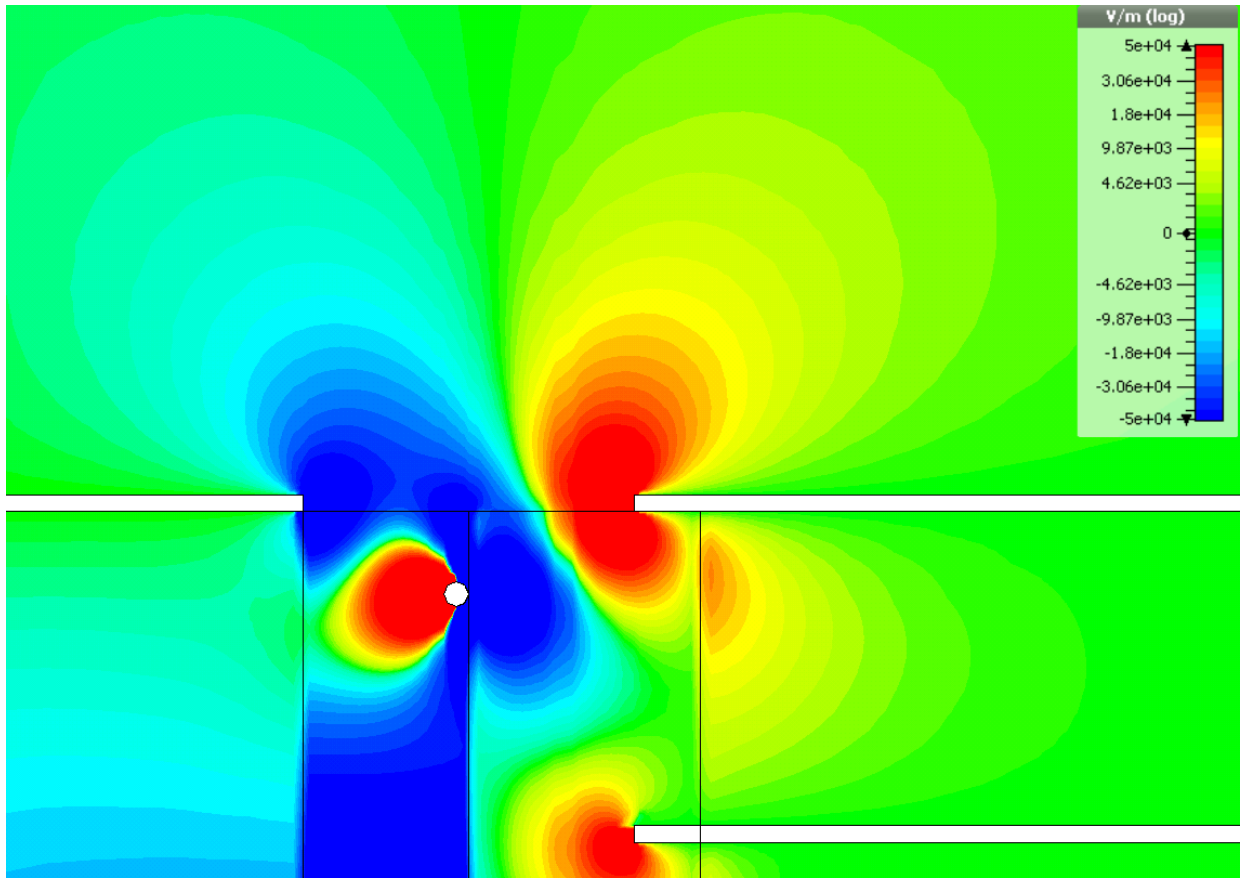

Figure 13: Difference between the default readout module and modified versions of the readout module. Shown is the collection efficiency on row 1.
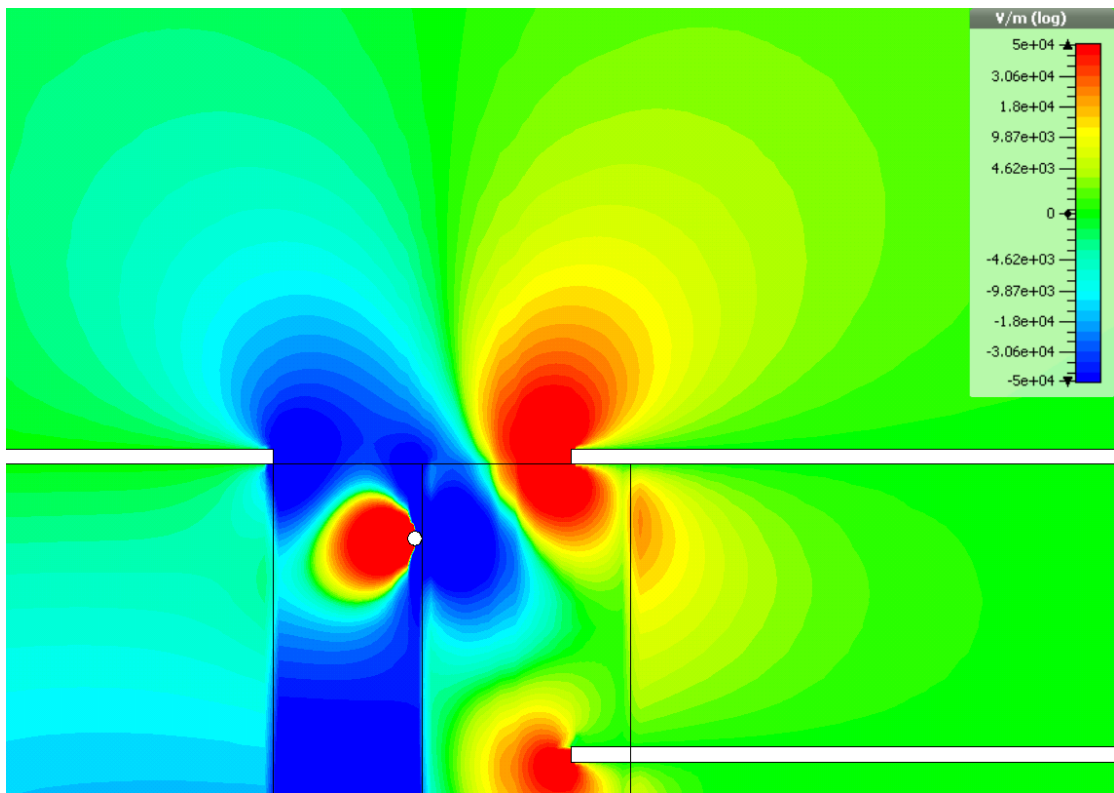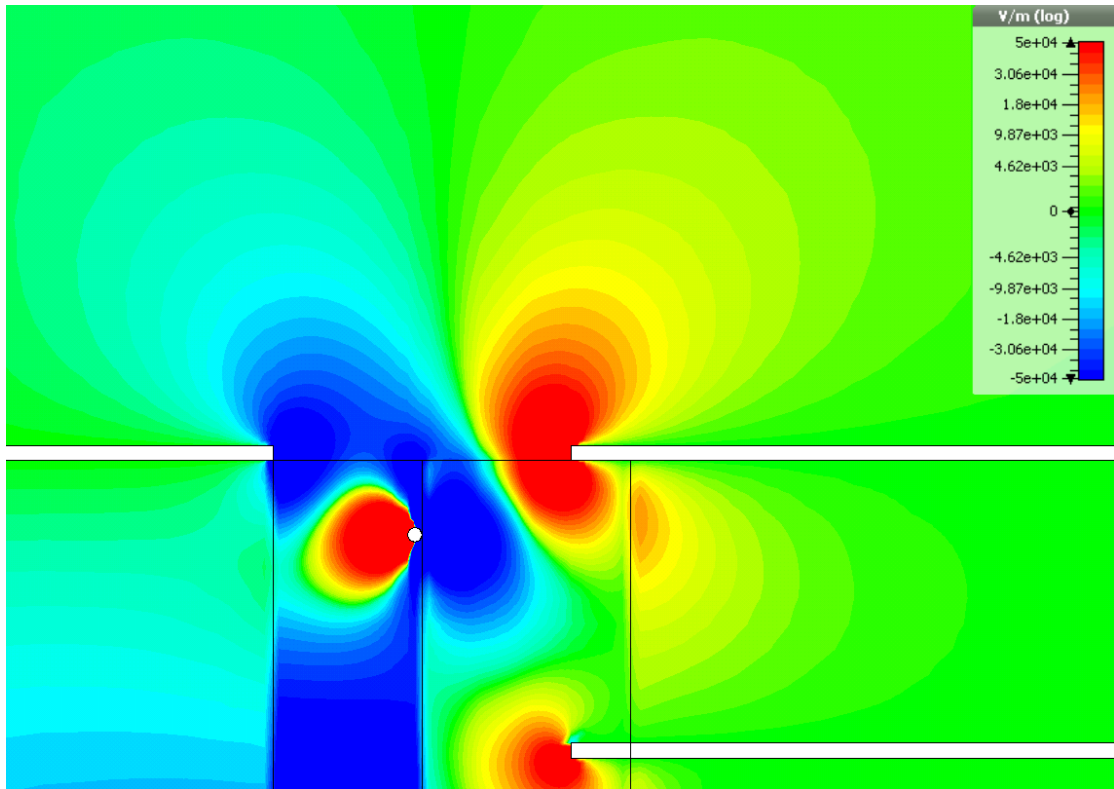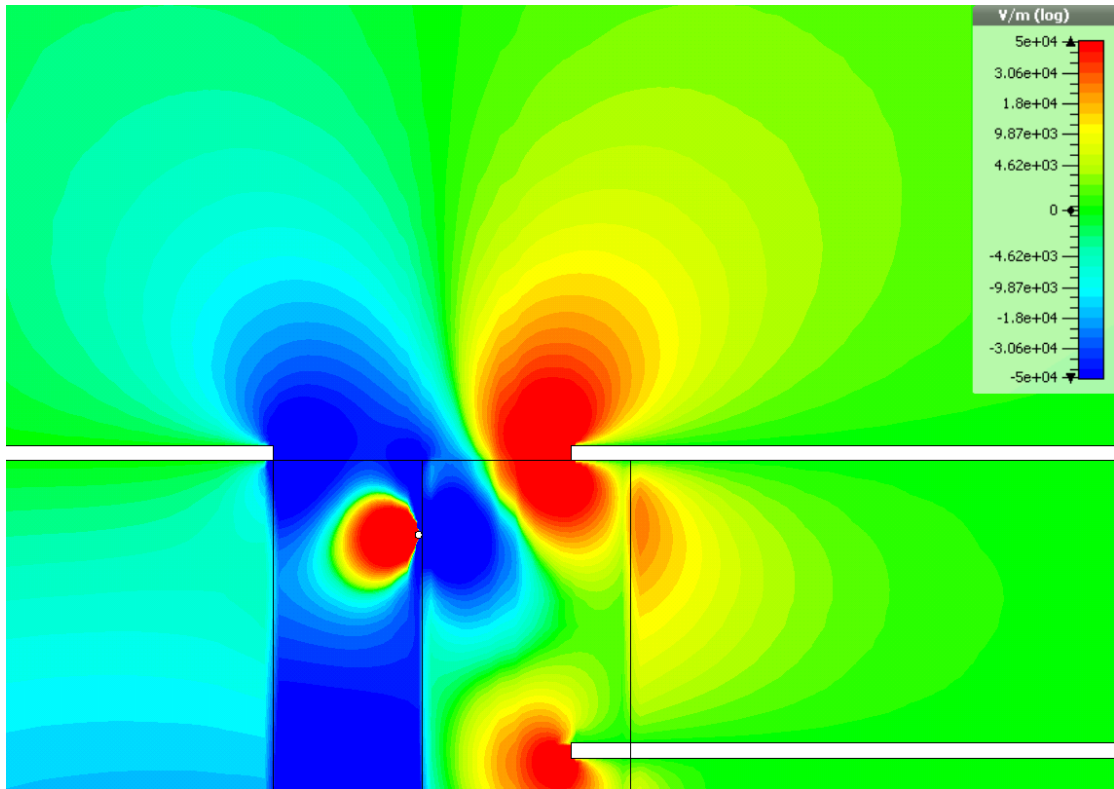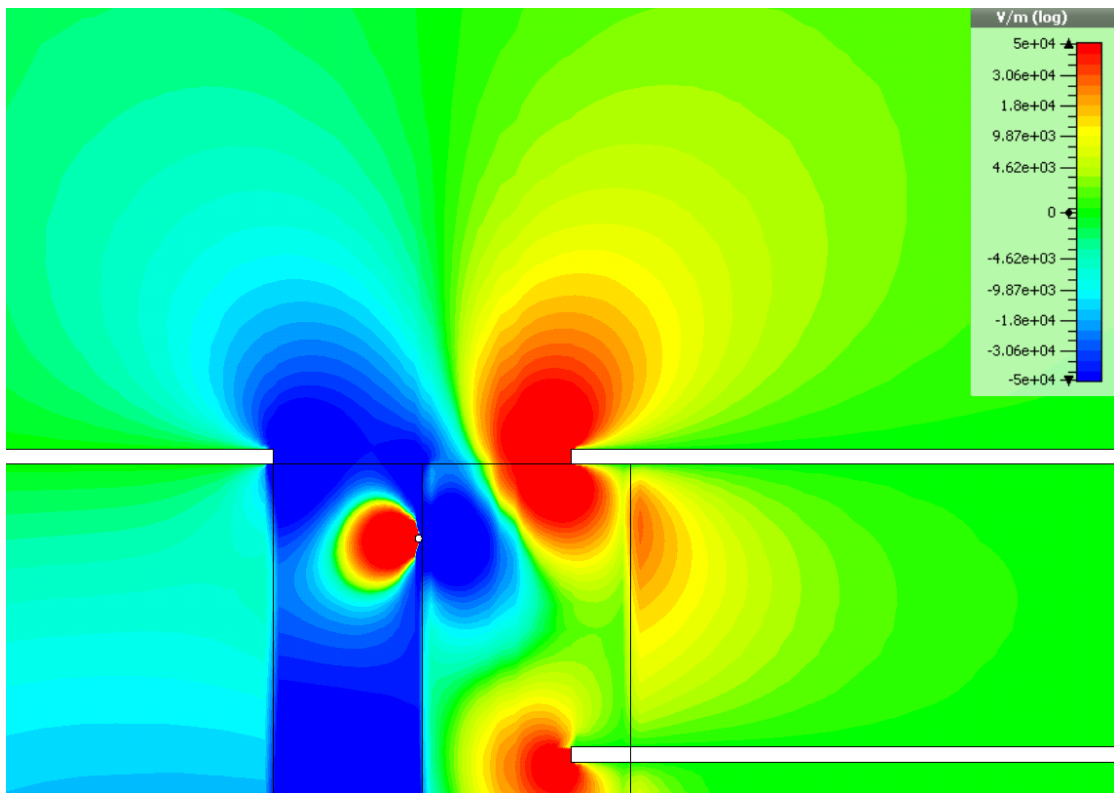
Acknowledgements

A   Results of the field simulations

Figure 14: Electric field transverse to the drift field for the readout module with a wire (150 µm) attached at a potential of $U_{\mathrm{wire}} = -2189\,\mathrm{V}$.

(a) Readout module with a wire (100 µm) attached at a potential of $U_{\text{wire}} = -2200\,\text{V}$.

(b) Readout module with a wire (100 µm) attached at a potential of $U_{\text{wire}} = -2189\,\text{V}$.

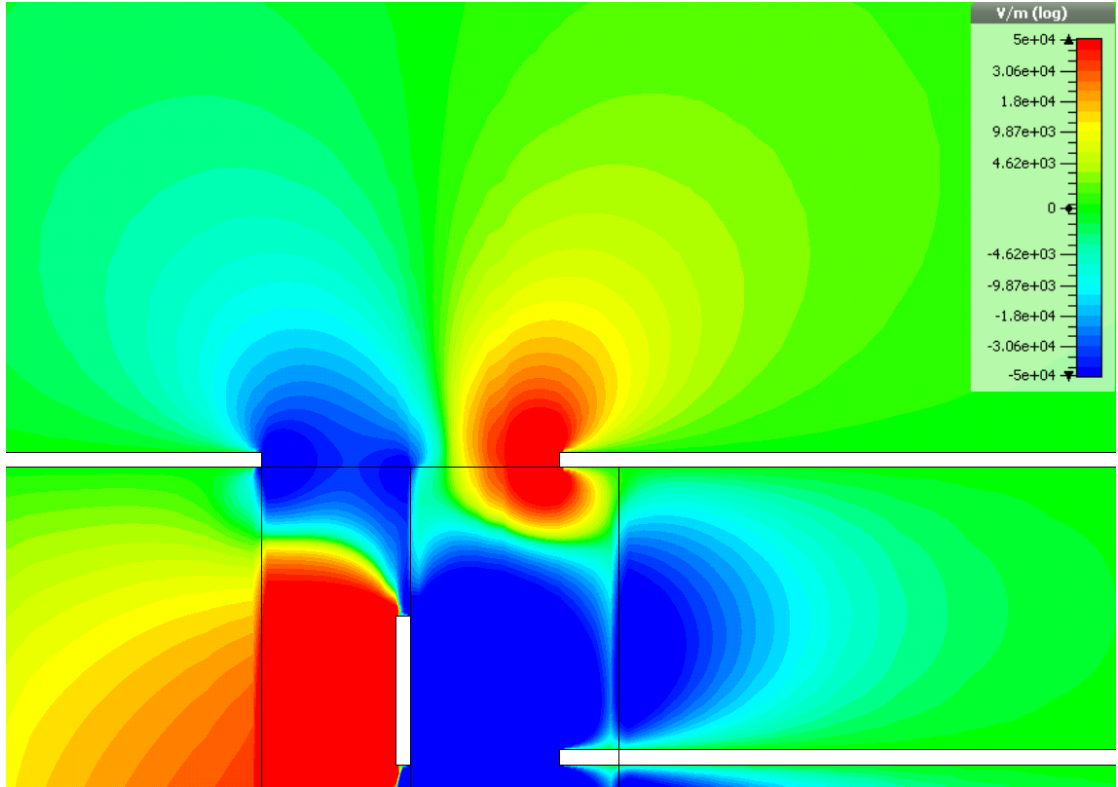**Figure 15:** Electric field transverse to the drift field for the readout module with a wire (100 µm) attached.

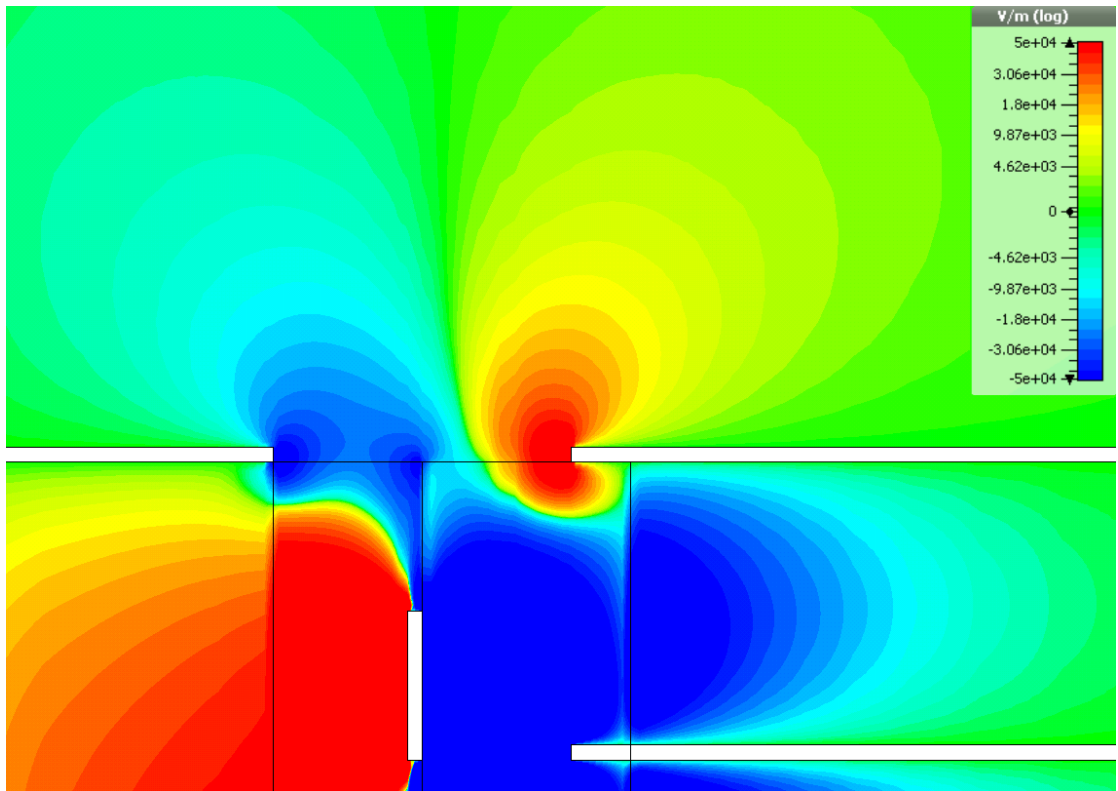(a) Readout module with a wire (50 µm) attached at a potential of $U_{\mathrm{wire}} = -2200\,\mathrm{V}$.

(b) Readout module with a wire (50 µm) attached at a potential of $U_{\mathrm{wire}} = -2189\,\mathrm{V}$.

Figure 16: Electric field transverse to the drift field for the readout module with a wire (50 µm) attached.

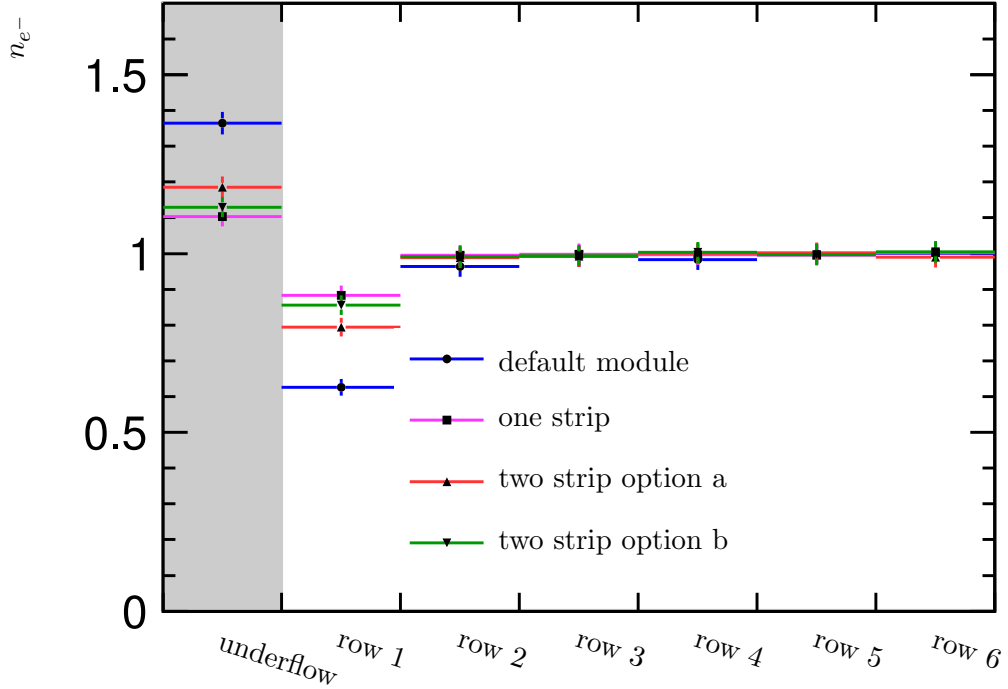(a) Readout module with two strips at a potential of $U_{\text{strip},1} = -2167\,\text{V}$ and $U_{\text{strip},2} = -2123\,\text{V}$ respectively.

(b) Readout module with two strips at a potential of $U_{\text{strip},1} = -2233\,\text{V}$ and $U_{\text{strip},2} = -2277\,\text{V}$ respectively.

**Figure 17:** Electric field transverse to the drift field for the readout module with two strips attached.

B   Summary of the drift study results

Table 3: Different wire and strip options and the corresponding number of electron endpoints on row 1 normalised to row 6.
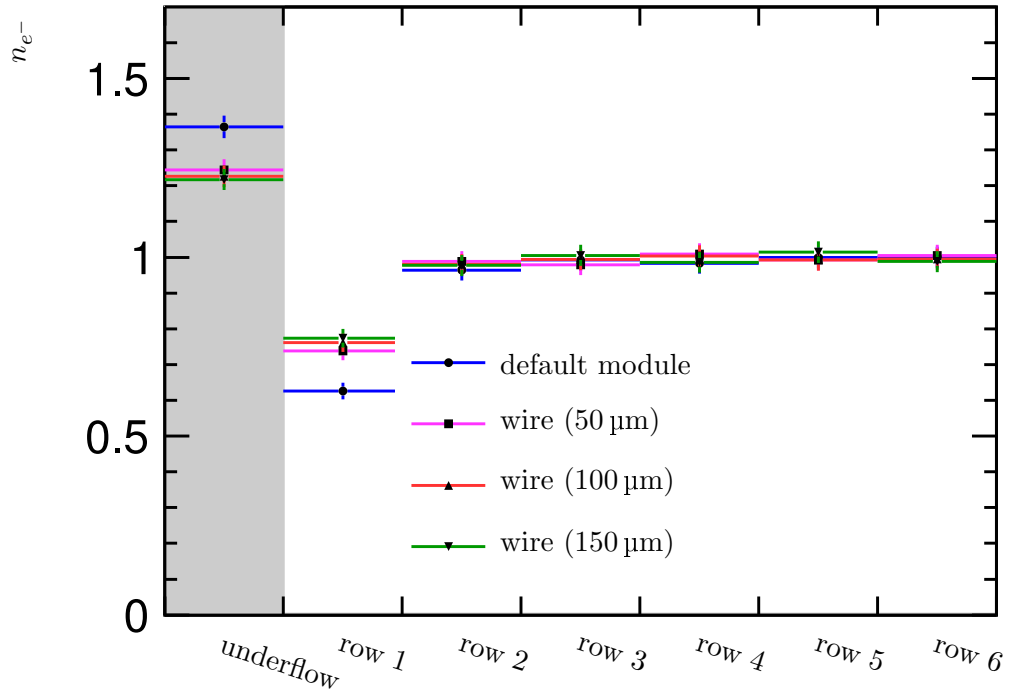
	n_{e^-} [%]	
	option a	option b
wire ($d = 50\,\mu\text{m}$)	73.4 ± 2.6	74.5 ± 2.5
wire ($d = 100\,\mu\text{m}$)	77.2 ± 2.6	75.0 ± 2.5
wire ($d = 150\,\mu\text{m}$)	78.1 ± 2.6	76.0 ± 2.5
one strip	87.9 ± 2.9	
two strips:	80.1 ± 2.6	85.5 ± 2.7

Figure 18: Number of electrons on a certain row position normalised to the expected number of electrons. Strips at different positions and potentials are attached to the readout module.
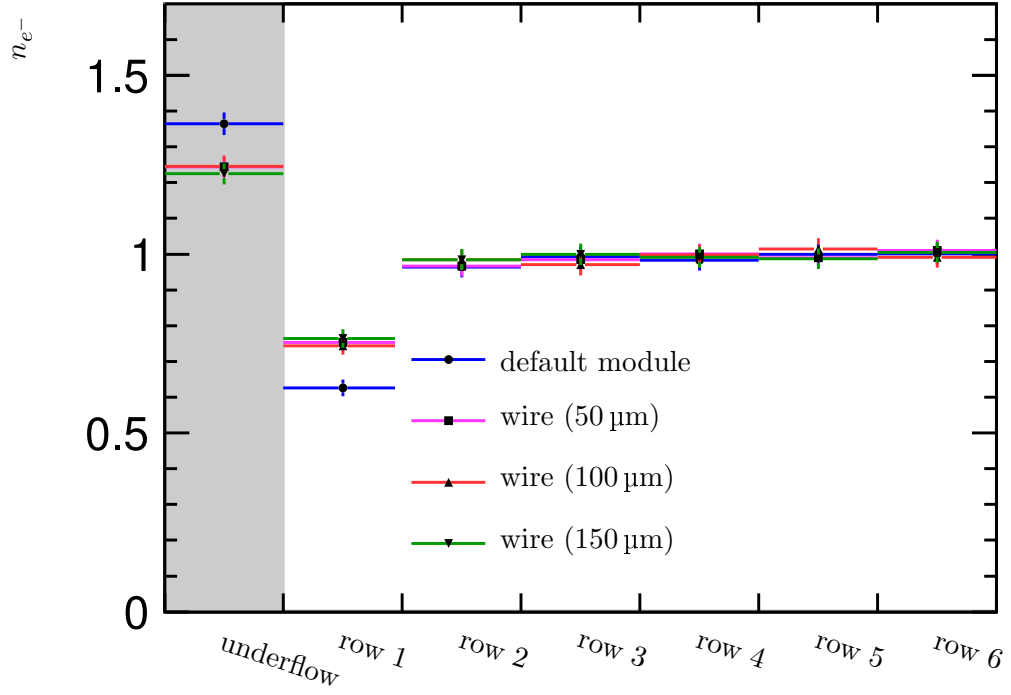
(a) The potential of the wire is $U_{\mathrm{wire}} = -2189\,\mathrm{V}$.

(b) The potential of the wire is $U_{\mathrm{wire}} = -2200\,\mathrm{V}$.

Figure 19: Number of electrons on a certain row position normalised to the expected number of electrons. Wires with different diameters are attached to the readout module.

References

[1] Klaus Dehmelt. Status of the Large TPC Prototype. *LCTPC Collaboration*, EUDET-Memo-2008-46, December 2008. `http://www.eudet.org/e26/e28/e615/e831/eudet-memo-2008-46.pdf`.

[2] R. Diener L. Steder T. Matsuda V. Prahl T. Behnke, K. Dehmelt and P. Schade. A lightweight field cage for a large TPC prototype for the ILC. *Journal of Instrumentation*, 5(10):P10011, 2010. doi: 10.1088/1748-0221/5/10/P10011.

[3] DESY test beam information. `http://adweb.desy.de/~testbeam/`.

[4] F. Sauli. Gem: A new concept for electron amplification in gas detectors. *Nuclear Instruments and Methods in Physics Research Section A: Accelerators, Spectrometers, Detectors and Associated Equipment*, 386(2–3):531 – 534, 1997.

[5] L. Hallermann. *Analysis of GEM Properties and Development of a GEM Support Structure for the ILD Time Projection Chamber*. PhD thesis, DESY, 2010.

[6] Jason Abernathy, Klaus Dehmelt, Ralf Diener, Jim Hunt, Matthias Enno Janssen, Martin Killenberg, Thorsten Krautscheid, Astrid Münnich, Martin Ummenhofer, Adrian Vogel, and Peter Wienemann. MarlinTPC: A marlin based common tpc software framework for the LC-TPC collaboration. *LCTPC Collaboration*, EUDET-Report-2007-04, October 2007.

[7] MarlinTPC project web page. `http://ilcsoft.desy.de/portal/software_packages/marlintpc`.

[8] CeramTech. `http://www.ceramtec.de/substrate/`.

[9] CST homepage. `www.cst.com`.

[10] M. Clemens and T. Weiland. Discrete electromagnetism with the finite integration technique. *Progress In Electromagnetics Research*, 32:65–87, 2001.

[11] B. Krietenstein, R. Schuhmann, P. Thoma, and T. Weiland. The perfect boundary approximation technique facing the big challenge of high precision field computation. In *Proceedings of the XIX International Linear Accelerator Conference (LINAC 98), Chicago, USA*, pages 860–862, 1998.

[12] Garfield++ project web page. `http://garfieldpp.web.cern.ch/garfieldpp/`.

[13] Garfield++ user guide, March 2012. `http://garfieldpp.web.cern.ch/garfieldpp/documentation/`.

[14] Magboltz project web page. `http://consult.cern.ch/writeup/magboltz/`.

[15] W. Blum and L. Rolandi. *Particle detection with drift chambers*. Accelerator physics. Springer-Verlag, 1993. ISBN 9783540583226.